Research Article

Journal of Environmental Nanotechnology

The Effect of Hydrothermal Reaction Time on the Antibacterial Activity of Synthesized Manganese Oxide Nanoparticles

R. Vaideeswaran[1], A. Yuvarani[1,3], I. Sophia Rani[2] and I. Reeta Mary[1*]

[1]Department of Physics, Government Arts College, Coimbatore, Tamilnadu, TN, India
[2]Department of Science and Humanities, Bharat Institute of Engineering and Technology, Hyderabad, TS, India
[3]Department of Physics, Nirmala College for Women, Coimbatore, TN, India
Received: 24.12.2023 Accepted: 27.12.2023 Published: 30.12.2023
*ireetamary@gmail.com

ABSTRACT

In the context of growing antibiotic resistance and the associated side effects of traditional antibiotics, this research explores the use of nanosized manganese oxide (Mn_3O_4) as a novel antibacterial agent. This study pioneers the synthesis of Mn_3O_4 through an eco-friendly hydrothermal method, varying reaction times (2, 4 and 6 hours) at a consistent temperature of 180 °C. Characterization techniques, including X-ray diffraction, Fourier-transform infrared spectroscopy and Scanning electron microscopy, provide insights into their crystallinity, functional groups and morphology. The synthesized Mn_3O_4 demonstrates remarkable antibacterial efficacy, with larger inhibition zones against both Gram-positive and Gram-negative strains compared to standard antibiotics. This research presents the synthesizing of an eco-friendly, cost-effective antibacterial agent through a straightforward hydrothermal method. Varying reaction times unveil distinctive antibacterial capabilities, making Mn_3O_4 a promising candidate for future antimicrobial systems and medical applications.

Keywords: Manganese oxide; Hydrothermal; Antibiotics; Antimicrobial; Medical applications.

1. INTRODUCTION

In recent years, the escalating resistance of bacteria to conventional drugs has driven the urgent need for alternatives. Current antibiotics designed to combat Methicillin-resistant *Staphylococcus aureus* (MRSA) and Vancomycin-resistant *S. aureus* (VRSA) often come at the cost of debilitating side effects, particularly to the gastrointestinal system (Amanda *et al*. 2020; Nitin *et al*. 2021). This pressing challenge has spurred a burgeoning interest in the synthesis of nanoparticles as a viable solution. However, while nanoparticle research is flourishing, relatively less attention has been directed towards materials that exhibit multiple oxidation states, with manganese (Mn) from transition metal oxides being a notable example (Duran and Seabra, 2012).

The manganese system unfolds a rich spectrum of crystallographic and stoichiometric phases, including α, β and γ, each linked to specific oxidation states. Of particular interest is the elusive hausmannite phase, attainable only at scorching temperatures exceeding 800 °C. Manganese oxide's potential extends far beyond its crystallographic versatility, setting it apart from other metal oxides ((Bhawana *et al*. 2011; Jayandran *et al*. 2015). Precise selection of transition metal oxides, such as CuO, ZnO, MnO and MgO has been considered as alternatives to traditional antibiotics. These metal oxides display a remarkable ability to harm pathogens by generating reactive oxygen species (ROS) with their higher oxidation potential. These ROS include singlet oxygen ($^1O_2$), hydroxyl radicals (.OH), and superoxide anion radicals ($.O_2^-$) (Xin *et al*. 2010; Shahriar *et al*. 2012).

In addition to its remarkable antibacterial properties, manganese oxide emerges as a promising candidate for diverse applications, from catalysis and sensor technology to anode materials for batteries. Moreover, it plays a pivotal role in redox reactions of aromatic hydrocarbons and features prominently in medicine, facilitating imaging techniques, biosensors, bio-remediation and drug carriers. Perhaps most intriguingly, manganese oxide has demonstrated an innate ability to inhibit bactericidal growth across various media (De *et al*. 2009).

The study conducted found that all species showed related inhibition towards nanoparticles, but the growth of *E. coli* is more retarded than *B. subtilis* (Mohan *et al*. 2016). Another group Bama Krishnan *et al*., established that composite clay/Mn_3O_4 nanoparticles showed better activity than pure clay which shows that ions of Mn_3O_4 are unbound, and penetrated through endo-cytoplasmic membranes of the strains *S. aureus, P. aeruginosa and C. albicans* (Bama and Sundrarajan, 2017). Wahran M. Saod *et al*. reported that combining commercial antibiotics with MnO nanoparticles

increased the efficiency of the antibiotics synthesized through plant extracts, due to the damage caused due to their small size and penetration that caused intracellular parts of the pathogens (Wahran *et al.* 2022).

In this study, Mn_3O_4 is synthesized using an eco-friendly hydrothermal method, employing precursors and NaOH. The investigation involved varying the reaction time (2, 4 and 6 h) while maintaining a consistent reaction temperature of 180 °C. X-ray diffraction (XRD) analysis revealed an average crystallite size of 15 ± 2 nm. Further characterization identified functional groups at 625 cm^{-1}, confirming the formation of Mn-O bonds in the tetragonal phase. Notably, Scanning electron microscopy (SEM) revealed the influence of reaction time on morphology. As the reaction time increased, nanoparticles emerged in well-dispersed formations, distinct from the initial clusters.

To assess the practicality of our synthesized Mn_3O_4, inhibition tests against specific pathogens were conducted, and results were compared with those obtained from standard antibiotics (Escarlata and Antonio, 2010; Subramanian *et al.* 2008; Virender *et al.* 2009). Encouragingly, the inhibition zones were notably larger for the samples subjected to a 6-hour reaction time. This promising outcome underscores the potential of Mn_3O_4 as an alternative to existing antibiotics, offering hope in the battle against drug-resistant bacteria.

2. MATERIALS AND METHODS

2.1 MATERIALS

Manganous acetate tetrahydrate from Hi-media, Sodium thiosulfate from Merck, Sodium hydroxide from Fisher Scientific and distilled water from Modern Scientific and Co., Coimbatore, India, were used as received.

2.2 SYNTHESIS OF Mn_3O_4 NANOPARTICLES

Manganese oxide nanoparticles were synthesized using a benign hydrothermal method with a constant temperature while varying the reaction times. Firstly, 0.1 M of Manganous acetate and 0.6 M of Sodium thiosulfate were added separately to 60 ml of distilled water. The mixtures were stirred vigorously with a magnetic stirrer for 30 minutes. Subsequently, the Sodium thiosulfate solution was introduced into the manganous acetate solution. The resulting mixture was allowed to stir further until homogeneity was achieved.

Then, 1 M of NaOH was added to the solution to raise the pH value to 12. The solution was stirred for an additional 30 minutes; then, the solution was sealed in a Teflon-lined stainless-steel autoclave and subjected to hydrothermal treatment for 2 hours at 180 °C. The solution was then allowed to cool gradually, and the settled precipitate was washed repeatedly with distilled water to remove impurities. The resulting precipitate was dried at 100 °C to obtain a brownish-black powder. The same series of reactions were repeated for 4 hours and 6 hours, respectively. Please refer to Fig. 1 for the experimental procedure.

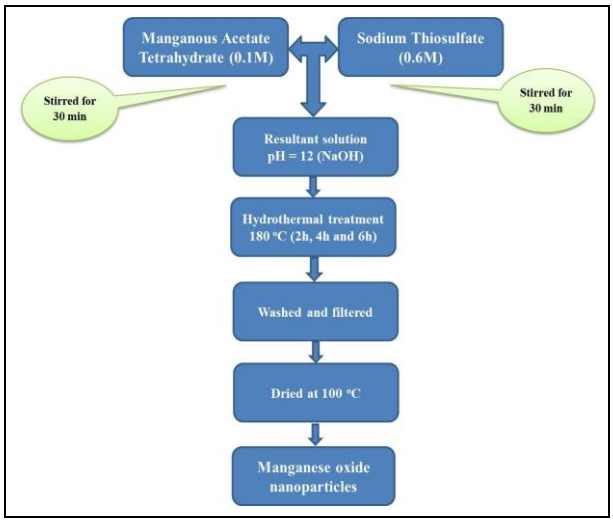

Fig. 1: Experimental flowchart

3. RESULTS AND DISCUSSION

3.1 CHARACTERIZATION OF Mn_3O_4 NANOPARTICLES

The synthesized samples were subjected to various characterization techniques to unveil their properties. X-ray diffraction (XRD) analysis was performed using a Rigaku Smart Lab X-ray diffractometer with Cu Kα radiation, maintaining 40 kV, to identify the crystalline phase. Fourier Transform Infrared Spectroscopy (FTIR) was conducted using a SHIMADZU Spectrophotometer. Additionally, the morphology of the samples was examined using a JEOL JSM 6390 LV Scanning Electron Microscope. Furthermore, the antimicrobial effects of the synthesized samples were evaluated against two pathogens: *Staphylococcus aureus* (*S. aureus*) and *Escherichia coli* (*E. coli*).

3.2 XRD ANALYSIS

The XRD patterns obtained for the prepared Mn_3O_4 nanoparticles are depicted in Fig. 1, with diffracted peaks aligning well with JCPDS card Number: 894837. The diffracted peak positions (2θ) were observed at 29.1°, 36.2°, 38.4°, 45.7°, 50.8°, 56.1°, 58.7°, 60.1° and 64.5°, corresponding to crystal planes (112), (103), (211), (220), (105), (303), (321), (224) and (400), respectively. Notably, the peaks at (103), (112), (211), and (224) appeared sharp and intense, confirming the tetragonal phase of the Mn_3O_4 nanoparticles. Crystallite

size calculations were performed using Scherrer's formula:

$$D = \frac{k\lambda}{\beta \cos\theta} \text{ (nm)}$$

where, D represents the crystallite size, k is the shape factor, λ is the X-ray wavelength of Cu Kα radiation, β is the full-width half maximum (FWHM) intensity in radians and θ is the Bragg's angle of the diffraction angle. The average crystallite size of Mn_3O_4 was found to be approximately 13, 13 and 15 nm for 2, 4 and 6 h of reaction time, respectively. It is noteworthy that the reaction time significantly influenced the average crystallite size of the nanoparticles. Up to 4 hours of reaction time, the nanoparticle size remained constant, while prolonged reaction time led to nanoparticle aggregation and an increase in particle size (Markides *et al.* 2012). The lattice constants for the tetragonal crystal system were calculated using the formula:

$$(a = b \neq c) \text{ and } (\alpha = \beta = \gamma = 90^o)$$

$$\frac{1}{d^2} = \frac{h^2 + k^2}{a^2} + \frac{l^2}{c^2}$$

Here, h, k and l represent Miller indices.

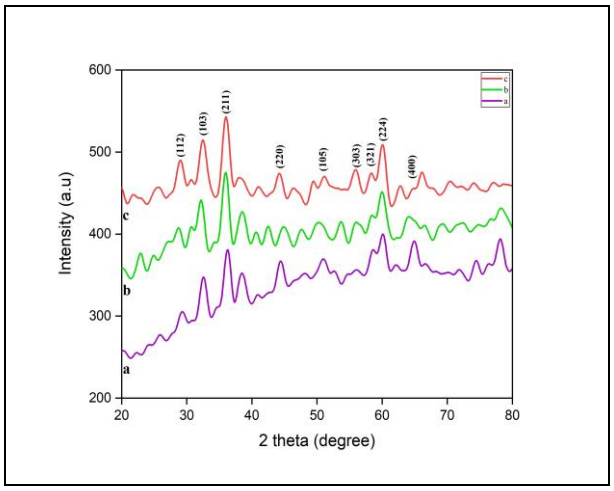

Fig. 2: XRD pattern of synthesized samples: (a) 2 h (b) 4 h and (c) 6 h

The increase in crystallite size from 13 to 15 nm as the reaction time extended from 2 to 6 h can be attributed to the decreasing pH of the solution over time. A lower pH level significantly contributes to an increase in particle size. Consequently, the reaction time plays a critical role in determining the size of the Mn_3O_4 nanoparticles formed at each stage, with the nanoparticle size increasing as the pH decreases with time (Celine *et al.* 2016).

Fig. 3 shows the FTIR spectra of the synthesized Mn_3O_4 samples after drying at 100 °C overnight. The significant peak observed at 625 cm^{-1} corresponds to the characteristic Mn-O stretching mode in the tetrahedral sites (Saeed *et al.* 2021). The peak at 2976 cm^{-1} is attributed to hydroxyl groups and water absorbed on the samples and the surface of the nanoparticles. Additionally, the peak at 1417 cm^{-1} is assigned to the acetate anions on the surface of the sample precipitate (Hee and Jinki, 2007). These observations and noted changes confirm that the chemical structure of the resultant products could be influenced by the addition of alkali during synthesis.

3.3 FTIR ANALYSIS

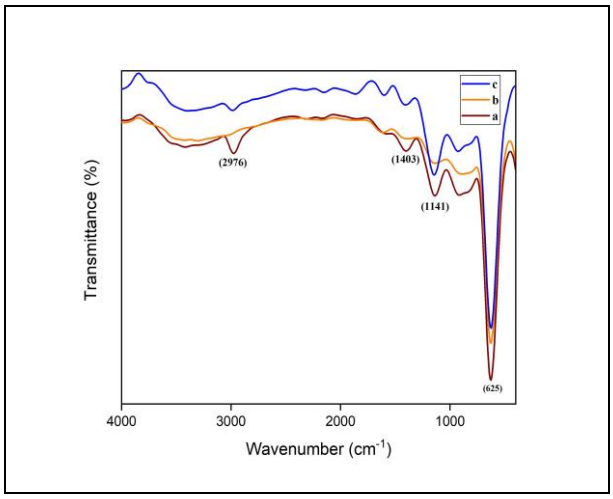

Fig. 3: FTIR spectra of synthesized samples: (a) 2 h (b) 4 h and (c) 6 h

3.4 SEM ANALYSIS

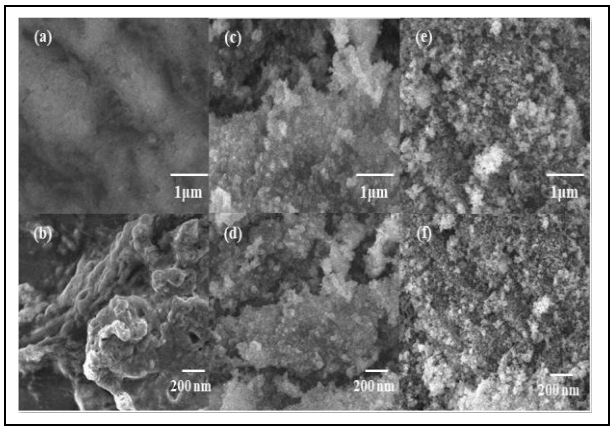

Fig. 4: SEM micrographs of synthesized samples: (a, b) 2 h, (c, d) 4 h and (e, f) 6 h

The surface morphologies of the synthesized samples were examined through SEM micrographs, as illustrated in Fig. 4, with two different magnifications: 1 mm and 200 nm, for the samples with reaction times of (a, b) 2 hours, (c, d) 4 hours, and (e, f) 6 hours, respectively. From the above micrographs, it is evident that the particles are very small and tend to agglomerate.

Initially, the particles are more agglomerated and less dispersed. However, as the reaction time increases to 4 h, the particles lose their tendency to agglomerate, leading to better dispersion over time. This is attributed to the homogeneous blending of precursors during the hydrothermal process, promoting particle dispersion (Hee and Jinki, 2007). The increase in particle size from 13 to 15 nm may be due to increased pressure over time and decreased particle growth due to coagulation among smaller nuclei. The increment in the size of individual particles contributes to the formation of multiple clusters, which in turn disperse well for a 6-hour reaction time (Amro *et la.* 2011).

4. APPLICATION STUDY

4.1 ANTIBACTERIAL ACTIVITY

4.1.1 Inoculum Preparation

Stock cultures were maintained at 4 °C on slopes of nutrient agar and potato dextrose agar. Active cultures for experiments were prepared by transferring a loopful of cells from stock cultures to test tubes containing 50 ml of nutrient broth. Bacterial cultures were incubated with agitation for 24 h at 37 °C in a shaking incubator, while fungal cultures were incubated at 27 °C for 3-5 days. Each suspension of the test organism was subsequently streaked onto nutrient agar media and potato dextrose agar. Bacterial cultures were then incubated at 37 °C for 24 hours, and fungal cultures were incubated at 27 °C for 3-5 days. A single colony was transferred to nutrient agar media slants and incubated at 37 °C for 24 h, while potato dextrose slants were incubated at 27 °C for 3-5 days. These stock cultures were stored at 4 °C. For use in experiments, a loopful of each test organism was transferred into 50 ml of nutrient broth and incubated separately at 37 °C for 18-20 h for bacterial cultures.

4.2 WELL DIFFUSION METHOD

The antibacterial and antifungal activities of crude extracts were determined using the Well Diffusion method (Bauer *et al.* 1996). For this, 2-20 µl of nanoparticle extract was added to the wells. The plates were then incubated at 37 °C for 24 h. The assay was conducted in triplicate, and control plates were also maintained. The zone of inhibition was measured from the edge of the well in mm. The tested cell suspension was spread on Muller-Hinton agar plates and potato dextrose agar. The well plates were then placed into the agar medium using sterile forceps. Plant extract was poured into the wells. The plates were incubated at 37 °C for approximately 24 h, and controls were also included. The zone of inhibition was measured from the clear zone in millimetres.

The antibacterial activity was performed using the agar diffusion method following Watt *et al*. (2001). The stock culture of bacteria (*E. coli and Staphylococcus aureus*) was obtained by inoculating nutrient broth media and incubating it at 37% for 18 h. Agar plates of the same media were prepared. Each plate was inoculated with 18-hour-old cultures, and the bacteria were swabbed onto sterile plates. The well was divided into 5 zones and filled with prepared sample solutions of 2 µl, 5 µl, 10 µl, 15 µl, and 20 µl, respectively. All the plates were incubated at 37 °C for 24 h; the diameter of the inhibition zone was measured in mm.

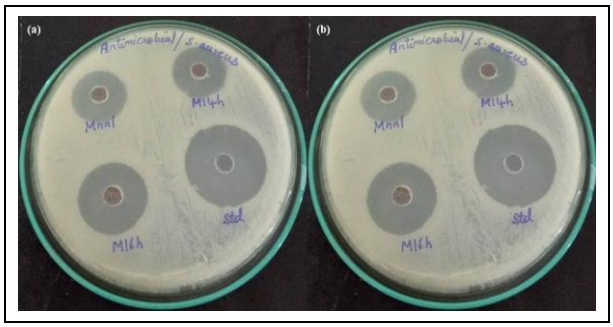

Fig. 5: Zone of inhibition: (a) *E. coli* and (b) *S. aureus*

Table 1. Zone of Inhibition compared with standard drug

Organism	Zone of Inhibition (mm)			
	Standard drug - Chloramphenicol (20 µl/disc)	Mn_3O_4 nanoparticles (20 µl/disc)		
		2 h	4 h	6 h
E. coli	9	4	5	16
S. aureus	10	7	8	25

From the figures and the results presented in Table 1, it can be concluded that the synthesized Mn_3O_4 samples exhibited antibacterial activity against both Gram-positive (*Staphylococcus aureus*) and Gram-negative (*Escherichia coli*) bacteria, which was compared to the standard antibiotic Chloramphenicol. There appeared to be a strong relationship between crystallite size and bactericidal effect. Typically, smaller nanoparticles showed better antibacterial activity than larger ones. However, in this case, the nanoparticles with increased crystallite size demonstrated good antibacterial activity. This suggests that size alone is not the only factor affecting bactericidal effect; the formulation and physical properties of the nanoparticles also play a role (Amro *et al.* 2011).

The generation of reactive oxygen species (ROS) is a result of defects in the nanoparticles, leading to the formation of impurity peaks that contribute to the generation of electron-hole pairs. During the hydrothermal reaction, which lasts for extended periods, such as 6 h, water molecules split, resulting in the formation of H+ and OH- ions. These ions eventually combine to form H_2O_2, which can penetrate the cell

membrane and disrupt cellular functions, inhibiting bacterial growth (Nagarajan and Rajagopalan, 2008).

CONCLUSION

This study was aimed at discovering a cost-effective antibacterial agent through a simple and eco-friendly hydrothermal method. Different reaction times (2, 4 and 6 h) were explored to assess antibacterial efficacy. FTIR spectral analysis confirmed the formation of Mn_3O_4 nanoparticles. Significant and distinct variations in morphology were observed for different reaction times. The crystallite sizes of the spherical nanoparticles were found to be approximately 13±2 nm. The results of the zone of inhibition assays demonstrated that the synthesized samples exhibited significant antibacterial activity against both Gram-positive and Gram-negative bacterial strains. This eco-friendly method shows promise and warrants further exploration in the field of antimicrobial systems and other potential medicinal applications in the future.

FUNDING

This research received no specific grant from any funding agency in the public, commercial or not-for-profit sectors.

CONFLICTS OF INTEREST

The authors declare that there is no conflict of interest.

REFERENCES

Amanda, C., Miren, E., Marta, E., Ana, L., Yolanda, C., Francesc, R., Elena, S., Antonio, C., Maria, L. G. and Eliana, B. S., State-of-the-art polymeric nanoparticles as promising therapeutic tools against human bacterial infections, *J. Nanobiotechnol.*, 18(1), 1-24 (2020). https://doi.org/10.1186/s12951-020-00714-2

Amro, M. E. B., Rendahandi, G. S., Brian, M., Kirk, G. S., Makram, T. S. and Thabet, M. T., Surface charge-dependent Toxicity of Silver nanoparticles, *Environ. Sci. Technol.*, 45(1), 283-287 (2011). https://doi.org/10.1021/es1034188

Bama, K. and Sundrarajan, M., Facile synthesis and antimicrobial activity of manganese oxide/bentonite nanocomposites, *Res. Chem. Intermed*., 43(4), 2351-2365 (2017). http://dx.doi.org/10.1007%2Fs11164-016-2765-7

Bauer, A. W., Kirby, W. M., Sherris, J. C. and Turck, M., Antibiotic susceptibility testing by a standardized single disk method, *Am. J. Clin. Pathol*., 45(4), 493-496 (2008). https://doi.org/10.1088/1468-6996/9/3/035004

Bhawana, Rupesh, K. B., Harpreet, S. B., Jain, V. K. and Nidhi, J., Curcumin nanoparticles: preparation, characterization, and antimicrobial study, J. Agric. Food Chem., 59(5), 2056-2061 (2011). https://doi.org/10.1021/jf104402t

Celine, R. I. R., Sathish, R., Jeya R. A. and Sagayaraj, P., Effect of reaction Time on Synthesis of Cadmium Selenide nanoparticles and the Efficiency of Solar cell, *J. Mater. Environ. Sci*., 7(5), 1589-1596 (2016).

De, Y., Pengxun, Y., Shuang, C., Jiangtao, C., Renfu, Z., Juanjuan, F. and Guangan, Z., Fabrication, In-Depth Characterization, and Formation Mechanism of Crystalline Porous Birnessite MnO2 Film with Amorphous Bottom Layers by Hydrothermal Method, *Cryst. Growth Des*., 9(1), 218-222 (2009). https://doi.org/10.1021/cg800312u

Duran, N. and Seabra, A. B., Metallic Oxide Nanopartilces: State of the Art in Biogenic Syntheses and Their Mechanisms, *Appl. Microbiol. Biotechnol.*, 95(2), 275-288 (2012). https://doi.org/10.1007/s00253-012-4118-9

Escarlata, R. C. and Antonio, V., Nanostructured bacterial materials for innovative medicines, *Trends Microbiol.*, 18(9), 423-430 (2010). https://doi.org/10.1016/j.tim.2010.06.007

Hee, D. J. and Jinki, J., The effects of Temperature on particle size in the Gas-Phase production of TiO2, *Aerosol Science and Technology*, 23(4), 553-560 (2007). https://doi.org/10.1080/02786829508965337

Jayandran, M., Muhamed, H. M. and Balasubramanian, V., Green synthesis and characterization of Manganese nanoparticles using natural plant extracts and its evaluation of antimicrobial activity, *J. Appl. Pharm. Sci.*, 5(12), 105-110 (2015). https://doi.org/10.7324/JAPS.2015.501218

Markides, H., Rotherham, M., and El, H. A. J., Biocompatibility and Toxicity of Magnetic nanoparticles in Regenerative Medicine, *J. Nanomater*., 2012(sp), 1-11 (2012). https://doi.org/10.1155/2012/614094

Mohan, K. K., Godavarthi, S., Vázquez, V. E., Casales, D. M., Mahendhiran, M., Hernandez, E. A., Syamala, R. M. G. and Martinez, G., Green synthesis of hausmannite nanocrystals and their photocatalytic dye degradation and antimicrobial studies, *J. Sol-Gel Sci. Technol.*, 80(2), 396-401 (2016). https://doi.org/10.1007/s10971-016-4136-7

Nagarajan, P. and Rajagopalan, V., Enhanced bioactivity of ZnO nanoparticles – an antimicrobial study, *Sci. Technol. Adv. Mater.*, 9(3), 1-7 (2008). https://doi.org/10.1088/1468-6996/9/3/035004

Nitin, C. T. D., Barbora, R., Jarmila, V. and Helena, B., Impact of Healthcare-Associated Infections Connected to Medical Devices-An Update, 9(11), 2332 (2021). https://doi.org/10.3390/microorganisms9112332

Saeed, Y., Ali, D., Abolee, D., Hardi, P., Joshua, S., Olivia, R., Ruihua, C., Afshin, I. and Amir, R. H., Model for Gold nanoparticle synthesis: Effect of pH and Reaction time, *ACS omega*, 6(26), 16847-16853(2021). https://doi.org/10.1021/acsomega.1c01418

Shahriar, S., Shahed, B., Sophie, L. and Laird, F. M., Pieter Stroevee and Morteza Mahmoudi, Toxicity of nanomaterials, *Chem. Soc. Rev*., 41(6), 2323-2343 (2012). https://doi.org/10.1039/C1CS15188F

Subramanian, V., Hongwei, Z. and Bingqing, W., Alcohol-assisted room temperature synthesis of different nanostructured manganese oxides and their pseudo-capacitance properties in neutral electrolyte, *Chem. Phys. Lett.*, 453(4), 242-249 (2008). https://doi.org/10.1016/j.cplett.2008.01.042

Virender, K. S., Ria, A. Y. and Yekaterina, L., Silver nanoparticles: Green synthesis and their antimicrobial activities, Advances in Colloid and Interface science, 145(1), 83-96 (2009). https://doi.org/10.1016/j.cis.2008.09.002

Wahran, M. S., Layth, L. H., Nisreen, J. A. and Asmiet, R., Biosynthesis and Antibacterial activity of manganese oxide nanoparticles prepared by green tea extract, *Biotechnol. Rep*., 34, e00729 (2022). https://doi.org/10.1016/j.btre.2022.e00729

Watt, E. V. D. and Pretorius, J. C., Purification and identification of active antibacterial components in Carpobrotus edulis L, *J. Ethnopharmacol.*, 6(1):87-91 (2001). https://doi.org/10.1016/s0378-8741(01)00197-0

Xin, L. and Jiao, S., Endothelial cells dysfunction induced by silica nanoparticles through oxidative stress via JNK/P53 and NF-kappaB pathways, *Biomater*., 31(32):8198-8209 (2010). https://doi.org/10.1016/j.biomaterials.2010.07.069